THE JOURNAL OF PHYSICAL CHEMISTRY B

Article

Cite This: J. Phys. Chem. B 2019, 123, 4929−4934

pubs.acs.org/JPCB

High-Field EPR Spectroscopic Characterization of Mn(II) Bound to the Bacterial Solute-Binding Proteins MntC and PsaA

Derek M. Gagnon,[†] Rose C. Hadley,[‡] Andrew Ozarowski,[§] Elizabeth M. Nolan,*[,‡] and R. David Britt*[,†]

[†]Department of Chemistry, University of California Davis, Davis, California 95616, United States

[‡]Department of Chemistry, Massachusetts Institute of Technology, Cambridge, Massachusetts 02139, United States

[§]National High Magnetic Field Laboratory, Florida State University, Tallahassee, Florida 32310, United States

Supporting Information

ABSTRACT: During infection, the bacterial pathogens *Staphylococcus aureus* and *Streptococcus pneumoniae* employ ATP-binding cassette (ABC) transporters to acquire Mn(II), an essential nutrient, from the host environment. Staphylococcal MntABC and streptococcal PsaABC attract the attention of the biophysical and bacterial pathogenesis communities because of their established importance during infection. Previous biophysical examination of Mn(II)-MntC and Mn(II)-PsaA using continuous-wave (≈9 GHz) electron paramagnetic resonance (EPR) spectroscopy revealed broad, difficult-to-interpret spectra (Hadley et al. *J. Am. Chem. Soc.* **2018**, *140*, 110−113). Herein, we employ high-frequency (>90 GHz), high-field (>3 T) EPR spectroscopy to investigate the Mn(II)-binding sites of these proteins and determine the spin Hamiltonian parameters. Our analyses demonstrate that the zero-field splitting (ZFS) is large for Mn(II)-MntC and Mn(II)-PsaA at +2.72 and +2.87 GHz, respectively. The measured ^{55}Mn hyperfine coupling values for Mn(II)-MntC and Mn(II)-PsaA of 241 and 236 MHz, respectively, demonstrate a more covalent interaction between Mn(II) and the protein compared to Mn(II) in aqueous solution (≈265 MHz). These studies indicate that MntC and PsaA bind Mn(II) in a similar coordination geometry. Comparison of the ZFS values determined herein with those ascertained for other Mn(II) proteins suggests that the Mn(II)-MntC and Mn(II)-PsaA coordination spheres are not five-coordinate in solution.

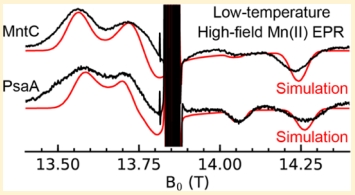

INTRODUCTION

Transition-metal ions are essential nutrients for all organisms.[1,2] In the context of bacterial infection, the invading microbe must acquire metal nutrients required for growth and virulence from the host.[2] These pathogens have evolved several mechanisms to scavenge and import metal ions that include the biosynthesis and deployment of metallophores and the expression of high-affinity metal-uptake proteins.[2] In this work, we employ high-field electron paramagnetic resonance (EPR) spectroscopy to evaluate the metal-binding properties of two transport proteins that function in the acquisition of Mn(II), a nutrient that is required for virulence in diverse bacterial pathogens.[3−5]

Staphylococcus aureus and *Streptococcus pneumoniae* are Gram-positive bacterial pathogens of significant clinical concern because they cause a variety of life-threatening infections.[6,7] Both organisms employ ATP-binding cassette (ABC) transporters to acquire Mn(II) from the host.[8,9] These transport systems consist of a membrane-anchored solute-binding protein (SBP) that scavenges Mn(II) from the extracellular environment, a transmembrane permease, and an ATPase located on the cytoplasmic side of the cell membrane.[10] The Mn(II) ABC transporters for *S. aureus* and *S. pneumoniae* are MntABC and PsaABC, respectively. MntC and PsaA are the SBPs that capture Mn(II) and deliver it to the transmembrane permeases of each uptake system.[11−13]

How MntC and PsaA coordinate Mn(II) and deliver it to their respective permease has not been fully elucidated. Reported crystal structures of Mn(II)-MntC (2.2 Å resolution)[14] and Mn(II)-PsaA (2.7 Å resolution)[15] show Mn(II) bound by a $His_2AspGlu$ coordination sphere in both proteins (Figure 1). The crystallographic Mn(II)-MntC site was described as five-coordinate where His50, His123, Oε1 of Glu189, and both Oδ1 and Oδ2 of Asp264 coordinate the metal ion (Figure 1B).[14] However, the metal−ligand distances determined crystallographically range from 2.1 to 2.8 Å and do not preclude the possibility of other coordination geometries (Figure 1). In addition, the metal content of the crystallized protein is ambiguous because the protein in solution contained low amounts of various metal ions according to inductively coupled-mass spectrometry and anomalous diffraction data were not reported,[14] which can be employed to confirm the identity of the bound metal. As a result, the Mn(II) coordination sphere of MntC is not well-defined and requires further examination. The crystallographic Mn(II)-PsaA site was described as four-coordinate where His67, His139, Oε1 of Glu205, and Oδ1 of Asp280 bind the Mn(II) ion (Figure 1D,E).[15] Nevertheless, the metal−ligand distances determined

Received: April 17, 2019
Revised: May 11, 2019
Published: May 22, 2019

DOI: 10.1021/acs.jpcb.9b03633
J. Phys. Chem. B 2019, 123, 4929−4934

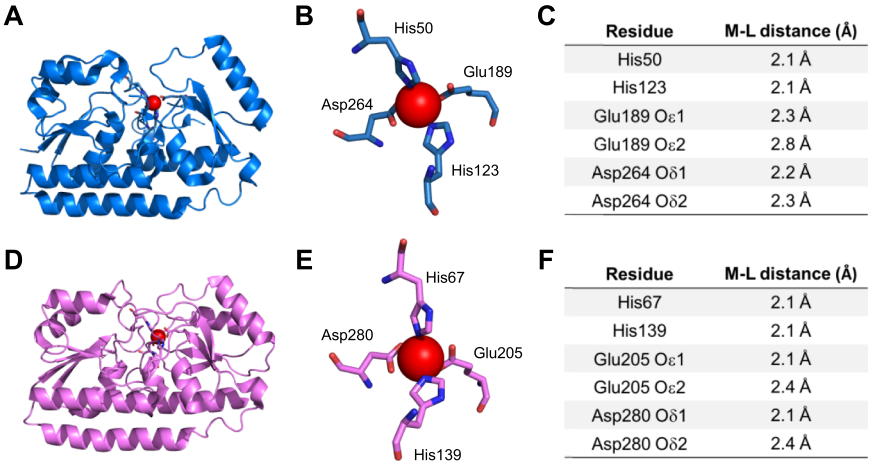

Residue	M-L distance (Å)
His50	2.1 Å
His123	2.1 Å
Glu189 Oε1	2.3 Å
Glu189 Oε2	2.8 Å
Asp264 Oδ1	2.2 Å
Asp264 Oδ2	2.3 Å

Residue	M-L distance (Å)
His67	2.1 Å
His139	2.1 Å
Glu205 Oε1	2.1 Å
Glu205 Oε2	2.4 Å
Asp280 Oδ1	2.1 Å
Asp280 Oδ2	2.4 Å

Figure 1. Crystal structures, zoom-in view of the metal-binding sites, and metal−ligand distances of Mn(II)-MntC (A−C; PDB: 4K3V) and Mn(II)-PsaA (D−F; PDB: 3ZTT). The Mn(II) ion is shown as a red sphere. Ligand numbering in MntC corresponds to a truncated form of the protein.[14]

from this crystal structure range from 2.1 to 2.4 Å,[15] and the possibility that the bound Mn(II) ion has a higher coordination number cannot be ruled out based on this structural model.[5] An additional consideration for each SBP is that the coordination geometry or number of the bound Mn(II) ion may change as the SBP delivers Mn(II) to the transmembrane permease. In an effort to gain further insight into these systems, we recently examined the Mn(II) sites of MntC and PsaA by X-band (≈9 GHz) EPR spectroscopy.[16] These studies revealed broad spectra resulting from the high magnitude of the zero-field splitting (ZFS) ($|D|$) relative to the spectrometer frequency ($|D|/h\nu \approx 0.3$).[16] As a consequence, the spin Hamiltonian parameters could not be accurately determined.

In this work, we further investigate the electronic structure of Mn(II)-MntC and Mn(II)-PsaA in the "high-field regime", where $|D| \ll h\nu$ by employing high-field (>3 T) and high-frequency (>90 GHz) EPR spectroscopy. In this regime, the spectra become simplified and simulation of the data can afford values for the spin Hamiltonian parameters. The spectral data and simulations indicate that both MntC and PsaA bind Mn(II) in a similar coordination environment consistent with the primary coordination sphere defined by the $His_2AspGlu$ motifs observed crystallographically.[14,15,17]

EXPERIMENTAL AND THEORETICAL METHODS

Sample Preparation. MntC and PsaA were overexpressed, purified, demetalated, and stored as described previously.[16] All EPR samples were buffer exchanged into 75 mM HEPES, 100 mM NaCl, pH 7.5, which was prepared using high-purity buffer reagents as described elsewhere.[16] For D-band analyses (130 GHz) of the Mn(II)-SBPs, samples of SBP (1 mM) were incubated with Mn(II) (750 μM) for ≈15 min before an approximately 15 μL aliquot was transferred to a D-band tube (0.50 × 0.60 mm ID × OD quartz capillary tubing supplied by VitroCom) and frozen in liquid nitrogen. These samples were prepared at MIT and shipped to the CalEPR facility at the University of California, Davis, in a liquid nitrogen dewar. For high-frequency (388 GHz) analyses, MntC (1.2 mM) was incubated with Mn(II) (900 μM) for ≈15 min before a 500 μL aliquot was transferred to a 1 mL low-density polyethylene (LDPE) sample vial (Fischer) and frozen in liquid nitrogen. PsaA (2.4 mM) was incubated with Mn(II) (1.8 mM) for ≈15 min before 500 μL was transferred to a 1 mL LDPE sample vial (Fischer) and frozen in liquid nitrogen. These samples were shipped to the National High Magnetic Field Laboratory (NHMFL) electron magnetic resonance facility on dry ice.

EPR Measurements. Pulse spectra at 130 GHz were collected at the University of California, Davis, CalEPR facility utilizing a D-band (130 GHz) spectrometer described previously.[18] Spectra were collected at 15 K, with a 20 ns $\pi/2$ pulse length, a τ value of 300 ns, and 1 ms repetition time. The field axis was calibrated by collecting the spectrum of Mn(II) impurity in MgO (>95% fused MgO, Aldrich). The Mn(II) in MgO has a g-value of 2.00100(5) and a ^{55}Mn hyperfine value of −243.6(5) MHz.[19,20]

Spectra collected at the NHMFL were collected utilizing a spectrometer described previously.[21] The field was calibrated with an internal sample standard of H-atom trapped in an octaisobutylsilsesquioxane nanocage with a g-value of 2.00294(3) and a hyperfine value of 1413.7(1) MHz.[19] Spectra were collected at multiple temperatures with different modulation amplitudes to enhance the intensity of different m_s transitions.

The field calibration with either the external Mn(II) impurity in MgO or the internal H-atom standards was carried out during postprocessing of the data. Briefly, the general procedure involved manually aligning a simulation of the standard with the experimental data of the field standard by both an initial visual inspection and a subsequent mathematical process. Example inputs for simulations of the standards are included in the Supporting Information. For the Mn(II) impurity in MgO standard, the lowest field hyperfine peak was selected for the initial alignment. After initial visual alignment, the fine adjustment was carried out by calculating the field difference between simulated and experimental field positions for the maximum intensity of the first hyperfine line. We found that this procedure afforded a satisfactory result where all six hyperfine lines of the Mn(II) impurity in MgO lined up. The calculated offset was then used as a field offset factor for the experimental data prior to simulation. The internal hydrogen atom standard required an entirely visual inspection alignment of the simulation and experimental data because of distortions of the line shape caused by passage and modulation effects during data collection.

DOI: 10.1021/acs.jpcb.9b03633
J. Phys. Chem. B 2019, 123, 4929−4934

EPR Theory and Simulations. The EPR spectrum of the d^5 Mn(II) ($S = 5/2$) ion can be interpreted using the phenomenological spin Hamiltonian given below.[22,23]

$$\hat{H} = \frac{\beta_e}{h} B \cdot g \cdot \hat{S} + a_{iso} \hat{S} \cdot \hat{I} + D(\hat{S_z}^2 - S(S+1)/3) + E(\hat{S_x}^2 - \hat{S_y}^2)$$

where β_e is the Bohr magneton, B is the magnetic field, g is the electron g-value, S is the electron spin, h is the Planck constant, a_{iso} is the isotropic hyperfine interaction with the ^{55}Mn ($I = 5/2$, 100% abundance) nucleus, I is the nuclear spin, and D and E are the axial and rhombic ZFS values, respectively. The ratio E/D is reported to indicate the rhombicity of the ZFS tensor. When the coordinate frame is chosen correctly, the values of E/D range from 0 (perfectly axial) to 1/3 (maximally rhombic). All spectra were simulated using the freely available EasySpin (v5.2.24) toolbox for MATLAB R2017a (The MathWorks, Inc.).[24]

The ^{55}Mn hyperfine values and g-values were determined from simulations of the data collected at temperatures ≥10 K and assessed by visual inspection. The ZFS values D and E were determined by simulating the data collected at temperatures ≤5 K. The asymmetry of the spectrum, from which the sign of D can be determined, depends on the magnitude of the Zeeman term rather than on the magnitude of D and is thus most convincingly observed at the lowest temperatures and highest fields. We found that the relative peak intensities of simulations at high fields and low temperature (≤5 K) were sensitive to the temperature employed in the simulation. In order to improve the agreement between the simulation and experimental data, it was necessary to set the simulation temperature 2 K higher than the temperature reported by the spectrometer to achieve the correct relative intensities of the different transitions. The simulation temperature is not expected to affect the measured ZFS parameters, but it affects the relative peak intensities in the simulations. The 388 and 400 GHz Mn(II)-MntC spectra collected at 3 K were simulated using a temperature of 5 K. The 388 GHz Mn(II)-PsaA spectrum collected at 5 K was simulated using a temperature of 7 K. We note that the recorded spectrometer temperature is not from a temperature probe located at the sample and that there may be heating of the sample induced by the field modulation during the experiment. D and E strains of 300 MHz were used to help the simulation line shape better match the line widths of the experimental data.

RESULTS AND DISCUSSION

The EPR spectra of Mn(II)-MntC and Mn(II)-PsaA feature a six-line pattern at $g \cong 2.001$ (4.64 T at 130 GHz, 13.86 T at 388 GHz) that arises from the transition between $m_s = \pm 1/2$ electron spin manifolds and their hyperfine couplings to the ^{55}Mn nucleus ($I = 5/2$, 100% abundance) (Figures 2–4 and S1). Surrounding this central sextet is a broad envelope of transitions belonging to the $m_s = \pm 3/2$ and $m_s = \pm 5/2$ manifolds where the ZFS and strain in these manifolds result in relatively featureless spectra with no resolved ^{55}Mn hyperfine couplings.[35] Simulation of the spectra in the sextet region affords ^{55}Mn isotropic hyperfine values of 241 and 236 MHz for Mn(II)-MntC and Mn(II)-PsaA, respectively (Table 1). The relatively low ^{55}Mn hyperfine constant values indicate a more covalent interaction of the $S = 5/2$ Mn(II) ion with its ligands in the binding site of the protein compared to hexaaqua Mn(II), for which the ^{55}Mn hyperfine value is ≈265 MHz.[22] This more covalent interaction and the electrostatic interaction from the negatively charged carboxylate groups of the $His_2AspGlu$ binding site likely contribute to the tight binding of the Mn(II) ion ($K_{d,Mn(II)} \leq 10$ nM)[14,15] observed for these two proteins. The simulation also affords isotropic g-values of 2.0011 and 2.0007 for MntC and PsaA, respectively. The isotropic nature of g and the ^{55}Mn hyperfine is expected from the spherically symmetrical unpaired electron spin density of the high-spin ($S = 5/2$) d^5 ground state of the Mn(II) ion with no low-lying excited states.

The ZFS parameters D and E/D are best measured in the high-frequency/-field spectra. At these high fields and at low temperatures (<6 K), the lower Zeeman energy m_s −5/2 and −3/2 levels become preferentially populated, leading to an

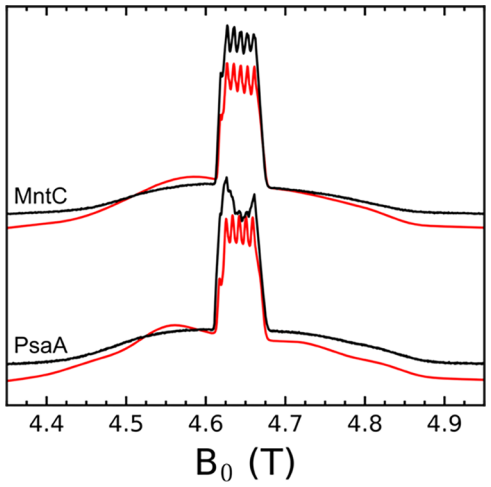

Figure 2. 2p echo-detected field sweep of Mn(II)-MntC and Mn(II)-PsaA at 130 GHz (75 mM HEPES, 100 mM NaCl, pH 7.5). The black traces are the experimental data, and the red traces are simulations with the parameters listed in Table 1. Experimental settings: spectrometer frequency 130 GHz, 1 ms rep time, 20 ns $\pi/2$ pulse length, τ = 300 ns, T = 15 K. The Mn(II)-PsaA spectrum appears to have a contaminant at ≈4.630–4.66 T that partially obscures the sextet.

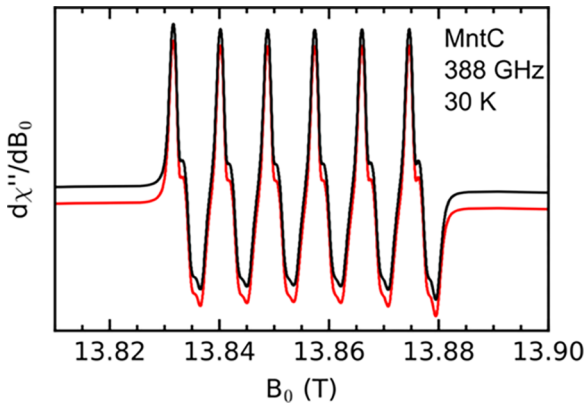

Figure 3. High-field/-frequency continuous-wave (CW) EPR spectrum of Mn(II)-MntC at 388 GHz (75 mM HEPES, 100 mM NaCl, pH 7.5). The black trace is the experimental data, and the red trace is a simulation with the parameters listed in Table 1. Experimental settings: spectrometer frequency 388 GHz, 0.5 mT modulation amplitude at 50 kHz, T = 30 K.

DOI: 10.1021/acs.jpcb.9b03633
J. Phys. Chem. B 2019, 123, 4929–4934

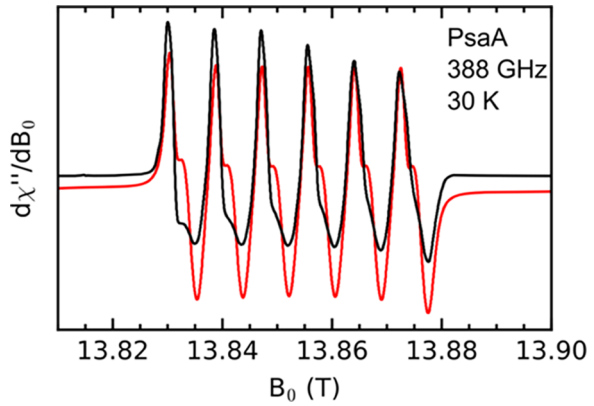

Figure 4. High-field/-frequency CW EPR spectrum of Mn(II)-PsaA at 388 GHz (75 mM HEPES, 100 mM NaCl, pH 7.5). The black trace is the experimental data, and the red trace is a simulation with the parameters listed in Table 1. Experimental settings: spectrometer frequency 388 GHz, 0.5 mT modulation amplitude at 50 kHz, T = 30 K.

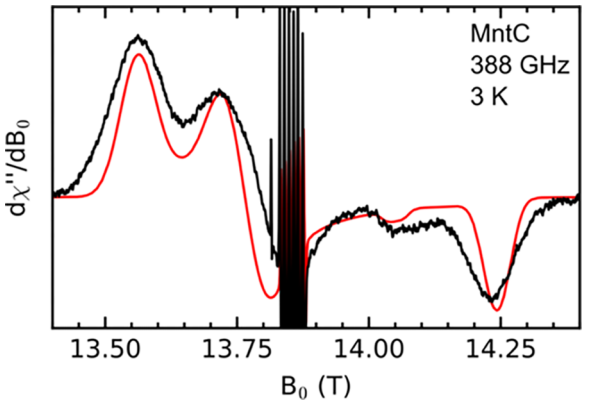

Figure 5. High-field/-frequency CW EPR spectrum of Mn(II)-MntC at T = 3 K, conditions where the spectrum is dominated by the −5/2 ↔ −3/2 and −3/2 ↔ −1/2 transitions (75 mM HEPES, 100 mM NaCl, pH 7.5). Experimental settings: spectrometer frequency 388 GHz, 2.5 mT modulation amplitude at 50 kHz, T = 3 K.

increased intensity of the m_s −5/2 ↔ −3/2 and −3/2 ↔ −1/2 transitions relative to the other transitions (Figures 5, 6, and S2). Simulation afforded values for D (E/D) of +2.72 GHz (0.177) and +2.87 GHz (0.122) for Mn(II)-MntC and Mn(II)-PsaA, respectively (Table 1). The ability to determine the magnitude and sign of D from high-field EPR spectroscopy allows comparisons to other spectroscopically and structurally characterized systems. The values of $|D|$ determined for Mn(II)-MntC and Mn(II)-PsaA are intermediate between the relatively high values reported for the five-coordinate superoxide dismutases (SODs) and the remarkably low values reported for the nearly idealized octahedral Mn(II) coordination spheres in human and murine calprotectin (Table 1).[26,33,34] Moreover, the sign of D is positive for the Mn(II)-SBPs and negative, when reported, for MnSOD.[25] Taken together, these comparisons suggest that the Mn(II)-SBP sites are neither five-coordinate nor highly symmetrical six-coordinate species. Moreover, the ZFS parameters for the Mn(II)-SBPs show the greatest similarity to the six-coordinate trigonal prismatic Mn(II) site displayed in OxDc site II and the six-coordinate bacterial reaction center from *Rhodobacter sphaeroides*.[27,28] Thus, it is possible that the Mn(II)-SBP sites are six-coordinate. However, we note that caution must be taken when using the magnitude of the Mn(II) ZFS parameter D to infer coordination geometry. The comparison should only be done with similar ligand types because the identity of the ligands can influence the ZFS.[36−38] We also note that there is a paucity of ZFS parameters determined for known tetrahedral Mn(II) complexes reported in the literature. To the best of our knowledge, this work is currently limited to Mn(II) complexes containing halide ligands,[39,40] which are inappropriate comparisons for the Mn(II)-SBPs because halide ligands affect the ZFS.[37−40] Thus, we are unable to determine how similar or

Table 1. Table of Spectroscopic Parameters for Mn(II) Bound to Various Proteins

Mn(II)-bound protein	D (GHz)[a]	$\|E\|$ (GHz)	$\|E/D\|$	^{55}Mn a_{iso}(MHz)	coordination motif[b]	refs
MntC	+2.72(5)	0.48(5)	0.177	241	N_2O_2 or N_2O_4	this work
PsaA	+2.87(5)	0.35(5)	0.122	236	N_2O_2 or N_2O_4	this work
Dr MnSOD[c]	−10.490	0.779	0.074	244	N_3O_2	25
Ec MnSOD[d]	10.640	0.853	0.080	230	N_3O_2	26
Ec MnSOD +0.1 M azide[d]	1.390	0.270	0.194	245	N_4O_2	26
Mn(II) photosynthetic reaction center from *R. sphaeroides*	3.328	0.749	0.225	n.d.[i]	N_4O_2	27
OxDc site I[e]	1.200	0.250	0.208	253	N_3O_3	28
OxDc site II[e]	2.700	0.675	0.250	250	N_3O_3	28
lipoxygenase[f]	+2.1−3	0.105−0.540	0.18(0.05)	258	N_3O_3	29,30
concanavalin A	0.645	0.071	0.010	259	N_1O_5	31
Mnx[g]	1.080	0.356	0.329	n.d.[i]	N_1O_5	32
human calprotectin	0.485	0.146	0.30	247	N_6	33
murine calprotectin	0.525	0.158	0.30	248	N_6	34
$[Mn(H_2O)_6]^{2+}$[h]	0.430−0.610	0−0.183	0−0.30	≈265	O_6	22

[a]The sign of D is unknown unless reported with a + or − sign. On the basis of uncertainty in the line widths, we estimate the error in our measurements to be ±50 MHz (±2.9 mT). [b]Nitrogen ligands are backbone amides, histidines, or azide. Oxygen ligands are carboxylate groups or water derived. The N_2O_2 and N_2O_4 motifs listed for MntC and PsaA are based on the current work. A N_2O_3 motif has been suggested for Mn(II)-bound MntC as described in the main text. [c]MnSOD of *Deinococcus radiodurans*. [d]MnSOD of *Escherichia coli*. [e]Oxalate decarboxylase of *Bacillus subtilis*. [f]Mn lipoxygenase from *Gaemannomyces grammis*. [g]Multicopper oxidase of *Bacillus* sp. PL-12 with the substrate Mn(II) bound. [h]The ZFS parameters and ^{55}Mn hyperfine for $[Mn(H_2O)_6]^{2+}$ depend on the ionic strength, buffer, and glassing agent as detailed in ref 22. [i]n.d. = not determined.

DOI: 10.1021/acs.jpcb.9b03633
J. Phys. Chem. B 2019, 123, 4929−4934

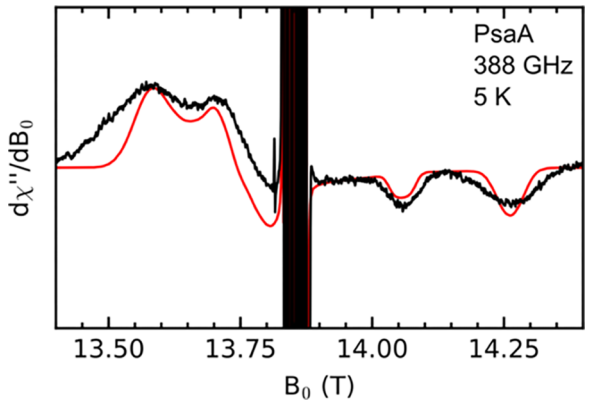

Figure 6. High-field/-frequency CW EPR spectrum of Mn(II)-MntC at T = 3 K, conditions where the spectrum is dominated by the −5/2 ↔ −3/2 and −3/2 ↔ −1/2 transitions (75 mM HEPES, 100 mM NaCl, pH 7.5). Experimental settings: spectrometer frequency 388 GHz, 2.4 mT modulation amplitude at 50 kHz, T = 5 K.

different the Mn(II) ZFS parameter values of the Mn(II)-SBPs are to other known tetrahedral Mn(II) species. Nevertheless, both Mn(II)-MntC and Mn(II)-PsaA exhibit similar spectroscopic parameters, which suggests that these two Mn(II) sites exhibit more similar coordination environments than indicated by interpretations and comparisons of the Mn(II)-MntC (five-coordinate)[14] and Mn(II)-PsaA (four-coordinate)[15] crystallographic data.

CONCLUSIONS

The high similarity in the spin Hamiltonian parameters determined for Mn(II)-MntC and Mn(II)-PsaA suggests that the Mn(II) coordination spheres of these two SBPs are nearly identical in solution. On the basis of comparisons to previously characterized Mn(II) proteins, the current data suggest that the Mn(II) sites of both proteins are not five-coordinate; however, more information on Mn(II) complexes of known coordination geometries is needed to further substantiate this possibility and ascertain whether the SBPs coordinate Mn(II) in a tetrahedral or six-coordinate environment. Thus, we reason that both SBPs release and deliver Mn(II) to their respective permeases in a similar manner. Indeed, elucidating the molecular basis for how the fully reconstituted transport systems capture Mn(II) and deliver the ion to the bacterial cytoplasm is an intriguing avenue for future investigation.

ASSOCIATED CONTENT

Supporting Information

The Supporting Information is available free of charge on the ACS Publications website at DOI: 10.1021/acs.jpcb.9b03633.

Figures S1 and S2, simulation parameters for field standards and EasySpin phenomenological line width inputs used in simulations (PDF)

AUTHOR INFORMATION

Corresponding Authors

*E-mail: lnolan@mit.edu Phone: 617-452-2495 (E.M.N).
*E-mail: rdbritt@ucdavis.edu Phone: 530-752-6377 (R.D.B).

ORCID

Derek M. Gagnon: 0000-0003-1737-6365
Andrew Ozarowski: 0000-0001-6225-9796
Elizabeth M. Nolan: 0000-0002-6153-8803
R. David Britt: 0000-0003-0889-8436

Notes

The authors declare no competing financial interest.

ACKNOWLEDGMENTS

We gratefully acknowledge financial support from the National Institute of Health grants R35GM126961 (R.D.B.) and R01GM118695 (E.M.N.). The work performed at the National High Magnetic Field Laboratory is supported by the National Science Foundation Cooperative Agreement no. DMR-1644779 and the State of Florida.

REFERENCES

(1) Waldron, K. J.; Rutherford, J. C.; Ford, D.; Robinson, N. J. Metalloproteins and metal sensing. *Nature* **2009**, *460*, 823−830.
(2) Hood, M. I.; Skaar, E. P. Nutritional immunity: transition metals at the pathogen-host interface. *Nat. Rev. Microbiol.* **2012**, *10*, 525−537.
(3) Papp-Wallace, K. M.; Maguire, M. E. Manganese transport and the role of manganese in virulence. *Annu. Rev. Microbiol.* **2006**, *60*, 187−209.
(4) Juttukonda, L. J.; Skaar, E. P. Manganese homeostasis and utilization in pathogenic bacteria. *Mol. Microbiol.* **2015**, *97*, 216−228.
(5) Brophy, M. B.; Nolan, E. M. Manganese and microbial pathogenesis: sequestration by the mammalian immune system and utilization by microorganisms. *ACS Chem. Biol.* **2015**, *10*, 641−651.
(6) Kobayashi, S. D.; Malachowa, N.; DeLeo, F. R. Pathogenesis of *Staphylococcus aureus* abscesses. *Am. J. Pathol.* **2015**, *185*, 1518−1527.
(7) Kim, L.; McGee, L.; Tomczyk, S.; Beall, B. Biological and epidemiological features of antibiotic-resistant *Streptococcus pneumoniae* in pre- and post-conjugate vaccine eras: a United States perspective. *Clin. Microbiol. Rev.* **2016**, *29*, 525−552.
(8) Horsburgh, M. J.; Wharton, S. J.; Cox, A. G.; Ingham, E.; Peacock, S.; Foster, S. J. MntR modulates expression of the PerR regulon and superoxide resistance in *Staphylococcus aureus* through control of manganese uptake. *Mol. Microbiol.* **2002**, *44*, 1269−1286.
(9) Dintilhac, A.; Alloing, G.; Granadel, C.; Claverys, J.-P. Competence and virulence of *Streptococcus pneumoniae*: Adc and PsaA mutants exhibit a requirement for Zn and Mn resulting from inactivation of putative ABC metal permeases. *Mol. Microbiol.* **1997**, *25*, 727−739.
(10) Ma, Z.; Jacobsen, F. E.; Giedroc, D. P. Coordination chemistry of bacterial metal transport and sensing. *Chem. Rev.* **2009**, *109*, 4644−4681.
(11) Rajam, G.; Anderton, J. M.; Carlone, G. M.; Sampson, J. S.; Ades, E. W. Pneumococcal surface adhesin A (PsaA): a review. *Crit. Rev. Microbiol.* **2008**, *34*, 131−142.
(12) Gribenko, A. V.; Liberator, P.; Anderson, A. S.; Matsuka, Y. V.; Mosyak, L. Cell surface antigen—manganese-binding protein MntC from *Staphylococcus aureus*. *Encyclopedia of Inorganic and Bioinorganic Chemistry*; John Wiley & Sons, Ltd., 2015.
(13) Eijkelkamp, B. A.; McDevitt, C. A.; Kitten, T. Manganese uptake and streptococcal virulence. *BioMetals* **2015**, *28*, 491−508.
(14) Gribenko, A.; Mosyak, L.; Ghosh, S.; Parris, K.; Svenson, K.; Moran, J.; Chu, L.; Li, S.; Liu, T.; Woods, V. L., Jr.; et al. Three-dimensional structure and biophysical characterization of *Staphylococcus aureus* cell surface antigen-manganese transporter MntC. *J. Mol. Biol.* **2013**, *425*, 3429−3445.
(15) McDevitt, C. A.; Ogunniyi, A. D.; Valkov, E.; Lawrence, M. C.; Kobe, B.; McEwan, A. G.; Paton, J. C. A molecular mechanism for bacterial susceptibility to zinc. *PLoS Pathog.* **2011**, *7*, e1002357.
(16) Hadley, R. C.; Gagnon, D. M.; Brophy, M. B.; Gu, Y.; Nakashige, T. G.; Britt, R. D.; Nolan, E. M. Biochemical and spectroscopic observation of Mn(II) sequestration from bacterial Mn(II) transport machinery by calprotectin. *J. Am. Chem. Soc.* **2018**, *140*, 110−113.

DOI: 10.1021/acs.jpcb.9b03633
J. Phys. Chem. B 2019, 123, 4929−4934

(17) Lawrence, M. C.; Pilling, P. A.; Epa, V. C.; Berry, A. M.; Ogunniyi, A. D.; Paton, J. C. The crystal structure of pneumococcal surface antigen PsaA reveals a metal-binding site and a novel structure for a putative ABC-type binding protein. *Structure* **1998**, *6*, 1553−1561.
(18) Oyala, P. H.; Ravichandran, K. R.; Funk, M. A.; Stucky, P. A.; Stich, T. A.; Drennan, C. L.; Britt, R. D.; Stubbe, J. Biophysical characterization of fluorotyrosine probes site-specifically incorporated into enzymes: *E. coli* ribonucleotide reductase as an example. *J. Am. Chem. Soc.* **2016**, *138*, 7951−7964.
(19) Stoll, S.; Ozarowski, A.; Britt, R. D.; Angerhofer, A. Atomic hydrogen as high-precision field standard for high-field EPR. *J. Magn. Reson.* **2010**, *207*, 158−163.
(20) Burghaus, O.; Rohrer, M.; Götzinger, T.; Plato, M.; Möbius, K. A novel high-field/high-frequency EPR and ENDOR spectrometer operating at 3 mm wavelength. *Meas. Sci. Technol.* **1992**, *3*, 765−774.
(21) Hassan, A. K.; Pardi, L. A.; Krzystek, J.; Sienkiewicz, A.; Goy, P.; Rohrer, M.; Brunel, L.-C. Ultrawide band multifrequency high-field EMR technique: a methodology for increasing spectroscopic information. *J. Magn. Reson.* **2000**, *142*, 300−312.
(22) Stich, T. A.; Lahiri, S.; Yeagle, G.; Dicus, M.; Brynda, M.; Gunn, A.; Aznar, C.; DeRose, V. J.; Britt, R. D. Multifrequency pulsed EPR studies of biologically relevant manganese(II) complexes. *Appl. Magn. Reson.* **2007**, *31*, 321−341.
(23) Weil, J. A.; Bolton, J. R. *Electron Paramagnetic Resonance: Elementary Theory and Practical Applications*, 2nd ed.; Wiley-Interscience: Hoboken, NJ, 2007.
(24) Stoll, S.; Schweiger, A. EasySpin, a comprehensive software package for spectral simulation and analysis in EPR. *J. Magn. Reson.* **2006**, *178*, 42−55.
(25) Sharma, A.; Gaidamakova, E. K.; Grichenko, O.; Matrosova, V. Y.; Hoeke, V.; Klimenkova, P.; Conze, I. H.; Volpe, R. P.; Tkavc, R.; Gostinčar, C.; et al. Across the tree of life, radiation resistance is governed by antioxidant Mn^{2+}, gauged by paramagnetic resonance. *Proc. Natl. Acad. Sci. U.S.A.* **2017**, *114*, E9253−E9260.
(26) Un, S.; Dorlet, P.; Voyard, G.; Tabares, L. C.; Cortez, N. High-field EPR characterization of manganese reconstituted superoxide dismutase from *Rhodobacter capsulatus*. *J. Am. Chem. Soc.* **2001**, *123*, 10123−10124.
(27) Tabares, L. C.; Cortez, N.; Agalidis, I.; Un, S. Temperature-dependent coordination in *E. coli* manganese superoxide dismutase. *J. Am. Chem. Soc.* **2005**, *127*, 6039−6047.
(28) Angerhofer, A.; Moomaw, E. W.; García-Rubio, I.; Ozarowski, A.; Krzystek, J.; Weber, R. T.; Richards, N. G. J. Multifrequency EPR studies on the Mn(II) centers of oxalate decarboxylase. *J. Phys. Chem. B* **2007**, *111*, 5043−5046.
(29) Gaffney, B. J.; Su, C.; Oliw, E. H. Assignment of EPR transitions in a manganese-containing lipoxygenase and prediction of local structure. *Appl. Magn. Reson.* **2001**, *21*, 413−424.
(30) Chen, Y.; Wennman, A.; Karkehabadi, S.; Engström, Å.; Oliw, E. H. Crystal structure of linoleate 13R-manganese lipoxygenase in complex with an adhesion protein. *J. Lipid Res.* **2016**, *57*, 1574−1588.
(31) Meirovitch, E.; Luz, Z.; Kalb, A. J. Electron spin resonance spectroscopy of aqueous solutions of concanavalin A. *J. Am. Chem. Soc.* **1974**, *96*, 7542−7546.
(32) Tao, L.; Stich, T. A.; Butterfield, C. N.; Romano, C. A.; Spiro, T. G.; Tebo, B. M.; Casey, W. H.; Britt, R. D. Mn(II) binding and subsequent oxidation by the multicopper oxidase MnxG investigated by electron paramagnetic resonance spectroscopy. *J. Am. Chem. Soc.* **2015**, *137*, 10563−10575.
(33) Gagnon, D. M.; Brophy, M. B.; Bowman, S. E. J.; Stich, T. A.; Drennan, C. L.; Britt, R. D.; Nolan, E. M. Manganese binding properties of human calprotectin under conditions of high and low calcium: X-ray crystallographic and advanced electron paramagnetic resonance spectroscopic analysis. *J. Am. Chem. Soc.* **2015**, *137*, 3004−3016.
(34) Hadley, R. C.; Gagnon, D. M.; Ozarowski, A.; Britt, R. D.; Nolan, E. M. Murine calprotectin coordinates Mn(II) at a hexahistidine site with Ca(II)-dependent affinity. *Inorg. Chem.* **2019**, DOI: 10.1021/acs.inorgchem.9b00763.
(35) Reed, G. H.; Markham, G. D. EPR of Mn(II) complexes with enzymes and other proteins. In *Biological Magnetic Resonance*; Berliner, L. J., Reuben, J., Eds.; Plenum Press: New York, 1984; Vol. *6*, pp 73−142.
(36) Walsby, C. J.; Telser, J.; Rigsby, R. E.; Armstrong, R. N.; Hoffman, B. M. Enzyme control of small-molecule coordination in FosA as revealed by ^{31}P pulsed ENDOR and ESE-EPR. *J. Am. Chem. Soc.* **2005**, *127*, 8310−8319.
(37) Duboc, C.; Phoeung, T.; Zein, S.; Pécaut, J.; Collomb, M.-N.; Neese, F. Origin of the zero-field splitting in mononuclear octahedral dihalide Mn^{II} complexes: an investigation by multifrequency high-field electron paramagnetic resonance and density functional theory. *Inorg. Chem.* **2007**, *46*, 4905−4916.
(38) Duboc, C.; Collomb, M.-N.; Neese, F. Understanding the zero-field splitting of mononuclear manganese(II) complexes from combined EPR spectroscopy and quantum chemistry. *Appl. Magn. Reson.* **2010**, *37*, 229−245.
(39) Wood, R. M.; Stucker, D. M.; Jones, L. M.; Lynch, W. B.; Misra, S. K.; Freed, J. H. An EPR study of some highly distorted tetrahedral manganese(II) complexes at high magnetic fields. *Inorg. Chem.* **1999**, *38*, 5384−5388.
(40) Zein, S.; Duboc, C.; Lubitz, W.; Neese, F. A systematic density functional study of the zero-field splitting in Mn(II) coordination compounds. *Inorg. Chem.* **2008**, *47*, 134−142.

DOI: 10.1021/acs.jpcb.9b03633
J. Phys. Chem. B 2019, 123, 4929−4934